remote sensing

MDPI

Article

An Integrated Framework for Spatiotemporally Merging Multi-Sources Precipitation Based on F-SVD and ConvLSTM

Sheng Sheng [1], Hua Chen [1,*], Kangling Lin [1], Nie Zhou [1], Bingru Tian [1] and Chong-Yu Xu [2]

[1] State Key Laboratory of Water Resources Engineering and Management, Wuhan University, Wuhan 430072, China; shengsheng@whu.edu.cn (S.S.); linkangling@whu.edu.cn (K.L.); niezhou@whu.edu.cn (N.Z.); tianbingru@whu.edu.cn (B.T.)
[2] Department of Geosciences, University of Oslo, P.O. Box 1047 Blindern, N-0316 Oslo, Norway; c.y.xu@geo.uio.no
* Correspondence: chua@whu.edu.cn

Abstract: To improve the accuracy and reliability of precipitation estimation, numerous models based on machine learning technology have been developed for integrating data from multiple sources. However, little attention has been paid to extracting the spatiotemporal correlation patterns between satellite products and rain gauge observations during the merging process. This paper focuses on this issue by proposing an integrated framework to generate an accurate and reliable spatiotemporal estimation of precipitation. The proposed framework integrates Funk-Singular Value Decomposition (F-SVD) in the recommender system to achieve the accurate spatial distribution of precipitation based on the spatiotemporal interpolation of rain gauge observations and Convolutional Long Short-Term Memory (ConvLSTM) to merge precipitation data from interpolation results and satellite observation through exploiting the spatiotemporal correlation pattern between them. The framework (FS-ConvLSTM) is utilized to obtain hourly precipitation merging data with a resolution of 0.1° in Jianxi Basin, southeast of China, from both rain gauge data and Global Precipitation Measurement (GPM) from 2006 to 2018. The LSTM and Inverse Distance Weighting (IDW) are constructed for comparison purposes. The results demonstrate that the framework could not only provide more accurate precipitation distribution but also achieve better stability and reliability. Compared with other models, it performs better in variation process description and rainfall capture capability, and the root mean square error (RSME) and probability of detection (POD) are improved by 63.6% and 22.9% from the original GPM, respectively. In addition, the merged precipitation combines the strength of different data while mitigating their weaknesses and has good agreement with observed precipitation in terms of magnitude and spatial distribution. Consequently, the proposed framework provides a valuable tool to improve the accuracy of precipitation estimation, which can have important implications for water resource management and natural disaster preparedness.

Keywords: spatiotemporal fusion; machine learning; multi-source precipitation; ConvLSTM; F-SVD

Citation: Sheng, S.; Chen, H.; Lin, K.; Zhou, N.; Tian, B.; Xu, C.-Y. An Integrated Framework for Spatiotemporally Merging Multi-Sources Precipitation Based on F-SVD and ConvLSTM. *Remote Sens.* **2023**, *15*, 3135. https://doi.org/10.3390/rs15123135

Academic Editor: Gwanggil Jeon

Received: 28 April 2023
Revised: 10 June 2023
Accepted: 13 June 2023
Published: 15 June 2023

1. Introduction

Precipitation is a critical meteorological variable with significant implications for many applications, including flood forecasting [1], agriculture [2], water resource management [3], and climate change studies [4]. Due to its large spatiotemporal variability, the accurate estimation of precipitation remains challenging, especially in areas with complex terrains and limited observational networks [5,6].

Traditional approaches to precipitation estimation rely on observations from rain gauges. These are simple devices that collect and measure the amount of precipitation. The observation data are usually considered reliable and accurate but have limited spatial coverage and are prone to errors due to gauge under-catch and exposure issues [7]. To overcome these limitations, many alternative approaches have been developed to estimate

precipitation, including remote sensing technologies such as radar and satellite [8]. Radar waves provide information on precipitation location, intensity, and distribution with a high temporal and spatial resolution. In contrast, satellite observations provide a large-scale view of precipitation with a relatively high spatial resolution but lower temporal resolution than radar waves [9]. Both offer improved spatial and temporal coverage, but the data may not be as accurate as that obtained from rain gauges. Therefore, combining data from multiple sources, also known as multi-source precipitation fusion, has become a promising way to overcome these limitations and provide more accurate estimates of precipitation.

In recent years, numerous statistical methods have been introduced for integrating precipitation data from rain gauges and satellites, including bias correction [10], Kriging-based methods [11], linear regression model [12], geographical difference analysis method [13], Bayesian combination method [14], Kalman filter calibration method [15], and geographically weighted regression method [16]. Duan et al. [17] merged the precipitation data observed at ground stations with the TRMM 3B42 satellite precipitation data by separately employing linear regression, geographically weighted regression, Kalman filer fusion, and the optimal interpolation method. The comparison results show that linear regression shows the best merging effect across the daily scale, while at the monthly scale, the precipitation data processed using the Kalman filter presented the highest accuracy. However, the aforementioned methodologies rely heavily on mathematical equations and strong assumptions, which can result in various limitations. Given the rapid advancement of machine learning (ML) technology, it possesses the potential to surmount certain limitations intrinsic to the aforementioned methods [18]. Unlike traditional approaches, ML exhibits more robust learning and generalization abilities, allowing it to effectively manage complex nonlinear relationships without requiring explicit statistical models. Additionally, ML demonstrates superior efficiency in processing vast amounts of data, thus enhancing its computational performance. Zhang et al. [19] used five ML algorithms (extreme gradient boosting, gradient boosting decision tree, random forest, LightGBM, and multiple linear regression) together with auxiliary geographic parameters to merge hourly data from meteorological stations, Radar, and satellites. The results show that the random forest-based hourly precipitation merging model is suitable for analyzing monsoon rainstorm events, while the extreme gradient boosting-based hourly precipitation merging model is suitable for analyzing typhoon events. Zhang et al. [20] applied four ML approaches, including a support vector machine, a random forest algorithm, an artificial neural network, and extreme gradient boosting, to construct the estimation models in which cloud properties are taken as additional predictors to improve the early run of the Integrated Multi-satellite Retrievals for GPM (IMERG).

Despite the progress in the development of multi-source precipitation merging models based on ML, most studies have primarily focused on describing the relationship be-tween the precipitation data and complex environment variables, while the spatiotemporal correlation patterns between satellite products and rain gauge observations have received relatively limited attention. The long short-term memory network (LSTM) is a type of recurrent neural network (RNN) specifically designed to handle long-term dependencies by utilizing a gating mechanism to regulate the flow of information. Shen et al. [21] proposed an integrated framework to merge multi-satellite and gauge precipitation data, which integrates the geographically weighted regression to improve the spatial resolution of precipitation estimations and the LSTM to improve the precipitation estimation accuracy by exploiting the temporal correlation pattern between multi-satellite precipitation products and rain gauges. Wu et al. [22] proposed a spatiotemporal deep fusion model by combining the convolutional neural networks (CNN) and the LSTM to merge the TRMM 3B42 V7 satellite data, rain gauge data, and thermal infrared images. The CNN was used to extract spatial features from the radar and satellite data, while the LSTM was used to capture the temporal features of the precipitation data. The superiority of LSTM in merging precipitation data has been verified. On the other hand, Convolutional LSTM (ConvLSTM) is an extension of LSTM that incorporates convolutional layers into its net-

work architecture, which allows it to perform spatiotemporal modeling of sequential data and capture spatiotemporal correlations more effectively due to its inherent convolutional structure. It has been successfully applied to precipitation nowcasting and verified to consistently outperform the fully connected LSTM [23]. To the best of our knowledge, there are no related studies merging satellite and gauge precipitation using a ConvLSTM network by formulating multi-source precipitation merging as a spatiotemporal sequence processing problem.

The purpose of our study is to address the challenge of spatiotemporally merging precipitation data from satellite and rain gauges by introducing an integrated framework. This framework aims to effectively combine spatiotemporal information from different data sources to enhance the accuracy and reliability of precipitation estimation. It integrates F-SVD in the recommender system to achieve the accurate spatial distribution of precipitation based on the spatiotemporal interpolation of rain gauge observations and ConvLSTM by exploiting the spatiotemporal correlation pattern between them. The framework (FS-ConvLSTM) is applied to the Jianxi Basin of China to generate hourly precipitation estimates with a resolution of 0.1° from the data of both rain gauges and GPM (IMERG V06) from 2006 to 2018.

2. Study Area and Materials

2.1. Study Area

The study area is located in the Jianxi basin in southeast China, between 117°31′–119°00′ east longitude and 26°31′–28°31′ north latitude (Figure 1). This basin is the largest tributary in the upper reaches of the Minjiang River, with its mainstream originating in Wuyishan and spanning 635.6 km. The entire drainage area of the Jianxi River basin covers 14,787 km^2, accounting for 27% of the total area of the Minjiang River basin. The basin is situated in a subtropical monsoon climate zone, characterized by humid air and abundant rainfall, with annual average rainfall ranging between 1800 and 2200 mm. Most rainfall occurs during the plum rain season from April to June and the typhoon rain season from July to September.

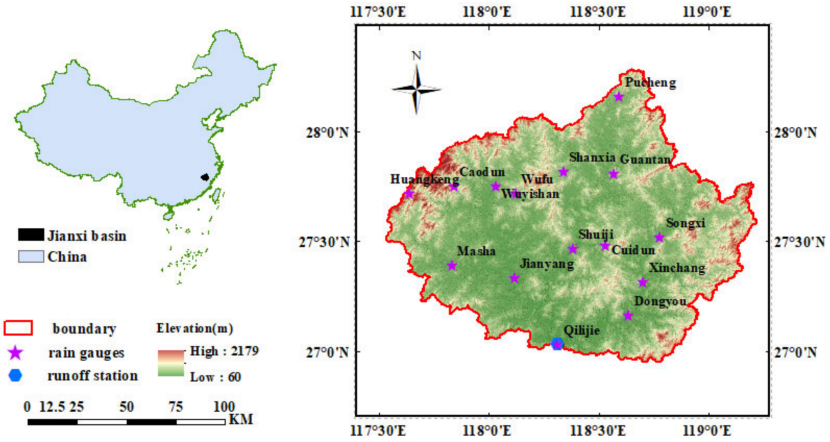

Figure 1. Location of the study area and spatial distribution of rain gauges.

2.2. Data

The network of rainfall gauges in the study area is characterized by its dense and evenly distributed nature, ensuring reliable data quality and high accuracy of the observations. The observation data used in this study were obtained from gauges operated by the Fujian Provincial Bureau of Hydrology, which are not classified as international exchange stations. The spatial distribution of meteorological stations can be seen in Figure 1, with a total of 15 rain gauges in the entire basin. Hourly data from 425 rainfall events from 2006 to 2018 were selected as the research data. The training period was from 2006 to 2014, and the testing period was from 2015 to 2018. The dataset was prepared through sliding windows,

resulting in a training set with a sample size of 272,916 and a test set with a sample size of 109,858.

To evaluate the accuracy improvement of the fusion model for different magnitudes of rainfall data, the maximum 12 h cumulative rainfall was calculated based on the selected 425 rainfall events. Rainfall was classified into four categories: light, moderate, heavy, and torrential, based on their magnitude as per the classification criteria listed in Table 1.

Table 1. Rainfall type classification criteria and results.

Type	Light	Moderate	Heavy	Torrential
Maximum 12 h rainfall (mm)	<5	5~15	15~30	>30
Number of events	6	157	160	102
Number of events in the training stage	4	102	112	79
Number of events in the testing stage	2	52	48	23

The satellite precipitation data were obtained from the Integrated Multi-Satellite Retrievals for Global Precipitation Measurement Mission (IMERG). Global Precipitation Measurement (GPM) is an international satellite mission conducted by the National Aeronautics and Space Administration (NASA) and Japan Aerospace Exploration Agency (JAXA), which uses multi-sensors, multi-satellites, and multi-algorithms combined with satellite networks and rain gauge inversion to obtain more accurate precipitation data. IMERG algorithm is designed to calibrate, combine, and interpolate satellite microwave precipitation estimates from the TRMM and GPM, as well as microwave-calibrated infrared satellite estimates, precipitation measurement analyses, and potentially other precipitation estimates. It has now been updated to product version V06B. This study uses GPM (IMERG V06) Final Run data with a spatial resolution of 0.1° and a temporal resolution of half an hour from January 2006 to December 2018 (https://earthdata.nasa.gov/; accessed on 15 October 2022).

3. Methodology

This study proposes an integrated framework to spatiotemporally merge precipitation data from rain gauge and GPM observations. Figure 2 presents the main structure of the framework: the spatiotemporal interpolation method based on F-SVD (Figure 2a) and the fusion model based on ConvLSTM (Figure 2b). The relevant methods are briefly described as follows.

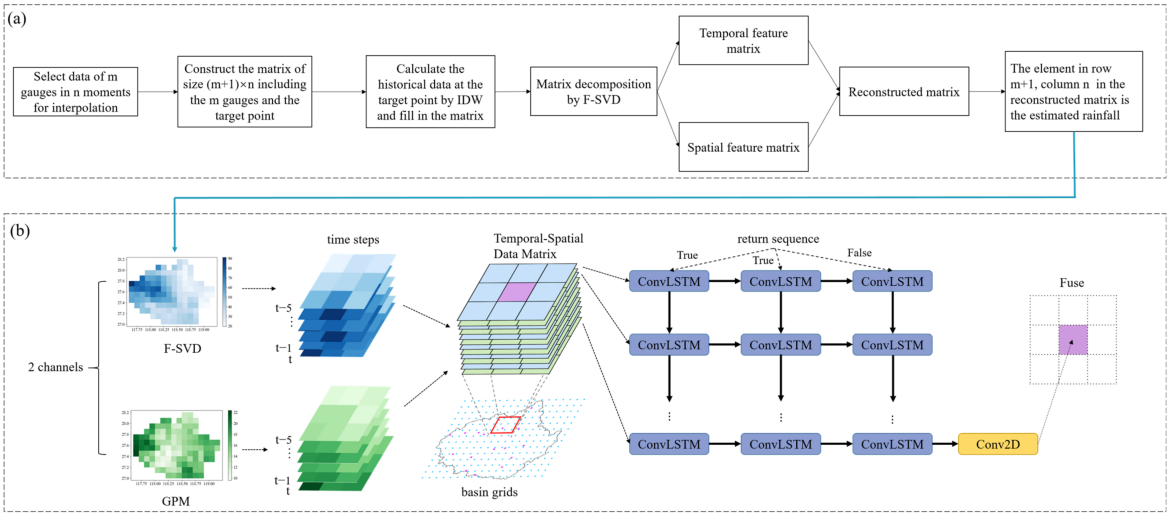

Figure 2. The integrated framework (FS-ConvLSTM) for the merging of precipitation data from rain gauge and GPM observations. (**a**) Spatiotemporal interpolation method based on F-SVD; (**b**) Fusion model based on ConvLSTM.

3.1. F-SVD

The interpolation method adopted in this study is a spatiotemporal precipitation method based on matrix decomposition (hereafter referred to as F-SVD) proposed by Chen et al. [24], which has been proven to outperform the traditional interpolation methods (inverse distance weight, ordinary kriging) through cross-validation and offer a better spatial estimation. The calculation process is presented in Figure 2a and contains the following steps:

(1) The historical precipitation information from m surrounding gauges and n past moments needs to be prepared for the interpolation at the target point at a certain moment.
(2) The precipitation data from the surrounding gauges and the target point from adjacent moments can form a spatiotemporal data matrix with dimensions of $(m+1) \times n$, where the rows represent time and columns represent space.
(3) If any precipitation values in the matrix representing the historical precipitation of the target point are unknown, traditional interpolation methods such as IDW should be used to calculate these values until only one null value representing the precipitation to be estimated remains.
(4) The F-SVD method is utilized to decompose the matrix into a temporal feature matrix X and a spatial feature matrix Y. The stochastic gradient descent algorithm is used for optimization.
(5) Then, the two optimal feature matrices are multiplied to reconstruct a matrix P, the element at the m + 1 row and n column in the reconstructed matrix represents the estimated precipitation, which is calculated as follows:

$$P_{\mathrm{i,j}} = \sum_{q=1}^{q} X_{\mathrm{i,q}} Y_{\mathrm{q,j}} \tag{1}$$

where q is the number of latent features.

3.2. ConvLSTM

ConvLSTM is an extension of LSTM, which uses convolutional layers to process spatiotemporal data [23]. It applies convolutions on the input data before passing it through the LSTM cells, allowing it to capture spatial and temporal dependencies within the input sequence [25]. As shown in Figure 3, the structure of ConvLSTM is similar to LSTM that contains forget gate (f_t), input gate (i_t), and output gate (O_t), but with convolutional layers instead of fully connected layers, which enables ConvLSTM to capture underlying spatial features [26]. The transmission relationship between the gates is expressed using the following equation:

$$i_t = \sigma(W_{xi} * \chi_t + W_{hi} * H_{t-1} + W_{ci} \circ C_{t-1} + b_i) \tag{2}$$

$$f_t = \sigma\left(W_{xf} * \chi_t + W_{hf} * H_{t-1} + W_{cf} \circ C_{t-1} + b_f\right) \tag{3}$$

$$C_t = f_t \circ C_{t-1} + i_t \circ \tanh(W_{xc} * \chi_t + W_{hc} * H_{t-1} + b_c) \tag{4}$$

$$o_t = \sigma(W_{xo} * \chi_t + W_{ho} * H_{t-1} + W_{co} \circ C_t + b_o) \tag{5}$$

$$H_t = o_t \circ \tanh(C_t) \tag{6}$$

where $\circ$ denotes the Hadamard product; $*$ denotes the convolution operator; σ is the sigmoid activation function, which is given by:

$$\sigma(x) = \frac{1}{1+e^{-x}} \tag{7}$$

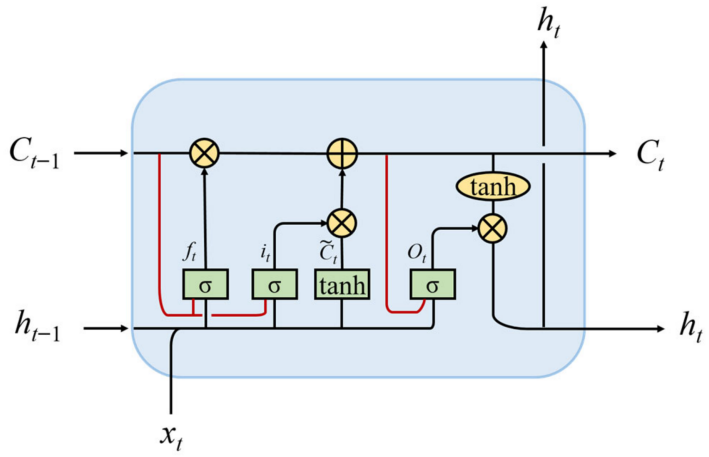

Figure 3. Structure of ConvLSTM cell.

3.3. The Spatiotemporal Fusion Model

The model diagram of the spatiotemporal fusion of precipitation data using ConvLSTM based on GPM satellite observation data and ground-based spatiotemporal interpolation data calculated by the F-SVD method is shown in Figure 2b.

At a point s in space, nine surrounding grid points, including itself, are selected to form the GPM satellite-observed precipitation matrix G^t and the ground spatiotemporal interpolated precipitation matrix I^t at time t. These matrices are defined as follows:

$$G^t = \begin{bmatrix} g_{s-4,t} & g_{s-3,t} & g_{s-2,t} \\ g_{s-1,t} & g_{s,t} & g_{s+1,t} \\ g_{s+2,t} & g_{s+3,t} & g_{s+4,t} \end{bmatrix}$$
$$I^t = \begin{bmatrix} i_{s-4,t} & i_{s-3,t} & i_{s-2,t} \\ i_{s-1,t} & i_{s,t} & i_{s+1,t} \\ i_{s+2,t} & i_{s+3,t} & i_{s+4,t} \end{bmatrix} \quad (8)$$

where $g_{s,t}$ and $i_{s,t}$ are the GPM satellite observation data and ground-based spatiotemporal interpolation data at time t, point s, respectively.

For the spatiotemporal precipitation fusion method, the GPM satellite observed precipitation matrix and the ground spatiotemporal interpolated precipitation matrix for the past six time periods need to be inputted into the constructed ConvLSTM to obtain the spatiotemporal fused precipitation $p_{s,t}$ at point s on space at time t in the following form:

$$p_{s,t} = f_{convlstm}\left[\left(G^{t-5}, G^{t-4}, \ldots, G^t\right), \left(I^{t-5}, I^{t-4}, \ldots, I^t\right)\right] \quad (9)$$

The structure of the ConvLSTM network model constructed for spatiotemporal precipitation fusion is presented in Figure 4. The figure illustrates the precipitation fusion process from input to output at a specific time point, with rectangles representing different neural network levels and rounded rectangles indicating the format of input, output, and intermediate variables. The input data have a tensor of size $6 \times 3 \times 3 \times 2$, where the dimensions represent time, row, column, and the number of channels, respectively. This tensor stores the data of GPM and ground-based spatiotemporal interpolation. The output data have a three-dimensional tensor of size $1 \times 1 \times 1$, with dimensions of time, rows, and columns, respectively, which holds the fused precipitation.

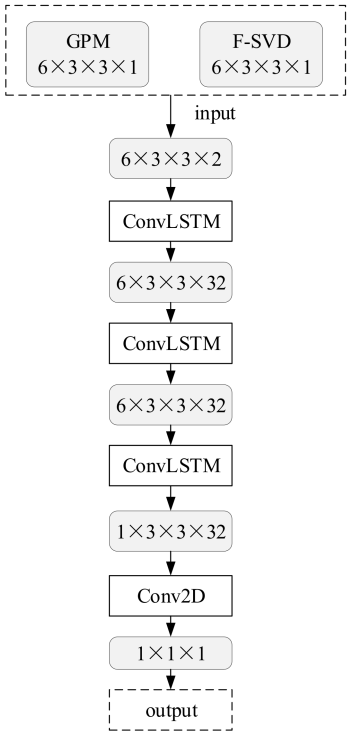

Figure 4. Structure of the three-layer ConvLSTM.

With the rain gauge as the central point, the nine surrounding grid points were selected. The input data for the ConvLSTM model comprised the GPM data and ground spatiotemporal interpolation data (F-SVD) of the past six moments, while the output was the precipitation observed at the station. The hourly precipitation data from 2006 to 2014 were used as the training set, and the hourly precipitation data from 2014 to 2018 were used as the testing set to evaluate the model's accuracy.

The main steps of the multi-source precipitation spatiotemporal fusion algorithm (FS-ConvLSTM) are as follows:

(1) Download GPM satellite observation data with a spatial resolution of 0.1° and a temporal resolution of 0.5 h. Process the data to obtain precipitation data with a time interval of 1 h.
(2) Collect and organize the rain gauge observation data of the study watershed and interpolate them into 0.1° × 0.1° spatial grid point data using the F-SVD method.
(3) Construct input sample sets based on GPM and interpolation results of F-SVD, normalize the data, and use the data from 2006 to 2014 as the training set and the data from 2014 to 2018 as the testing set.
(4) Train the model at 15 rain gauges with precipitation observations as the true value and mean squared error as the loss function to minimize the training loss.
(5) Apply the trained model to each grid point within the study watershed for precipitation fusion.

3.4. Evaluation Indicators

The quality of precipitation data is evaluated using two types of indices: quantitative and categorical. The quantitative evaluation index assesses factors such as rainfall magnitude and temporal distribution. It employs several measures, including relative deviation (*BIAS*), root mean square error (*RSME*), correlation coefficient (*CC*), and rainfall ratio (*RATIO*). Meanwhile, the categorical evaluation index focuses on the spatial distribution of

precipitation and uses probability of detection (*POD*), false alarm rate (*FAR*), threat score (*TS*), and missed alarm rate (*MAR*).

$$BIAS = \frac{\sum_{i=1}^{n} SAT_i - \sum_{i=1}^{n} OBS_i}{\sum_{i=1}^{n} OBS_i} \tag{10}$$

$$RSME = \sqrt{\frac{1}{n}\sum_{i=1}^{n} (SAT_i - OBS_i)^2} \tag{11}$$

$$CC = \frac{\sum_{i=1}^{n} \left(SAT_i - \overline{SAT}\right)\left(OBS_i - \overline{OBS}\right)}{\sqrt{\sum_{i=1}^{n} \left(SAT_i - \overline{SAT}\right)^2 \left(OBS_i - \overline{OBS}\right)^2}} \tag{12}$$

$$RATIO = \frac{\sum_{i=1}^{n} SAT_i}{\sum_{i=1}^{n} OBS_i} \tag{13}$$

$$POD = \frac{TP}{TP + FN} \tag{14}$$

$$FAR = \frac{FP}{TP + FP} \tag{15}$$

$$TS = \frac{TP}{TP + FN + FP} \tag{16}$$

$$MAR = \frac{FN}{FN + TP} \tag{17}$$

where n denotes the number of observation data; *SAT* and *OBS* refer to GPM observation and rain gauge observation, respectively; *TP* represents the number of accurately forecasted precipitation data; *FN* is the number of missed reports; and *FP* denotes the number of false reports. These variables are presented in Table 2. Specifically, *TP* indicates the number of precipitation data observed by both the satellite and the rain gauge, whereas *FP* refers to the number of precipitation data observed by the satellite but not by the rain gauge. On the other hand, *FN* represents the number of rainfall data observed by the rain gauge but not by the satellite.

Table 2. Description of TP, FP, FN, and TN.

Rain Gauge Observation	Satellite Product	
	Yes	**No**
Yes	TP	FN
No	FP	TN

4. Results

The study proposes an integrated framework (FS-ConvLSTM) and applies it to generate hourly spatial precipitation estimation through spatiotemporally merging data from rain gauge and GPM (IMERG V06) observations in the Jainxi basin of China from 2006 to 2018. The relevant results and findings are displayed in the following sub-sections: quality assessment on GPM (Section 4.1), accuracy evaluation of different models (Section 4.2), and model performance in typical rainfall events (Section 4.3).

4.1. Quality Assessment of GPM

The satellite rainfall observation dataset for the Jianxi watershed is constructed by collating GPM data at a 0.1° scale and 0.5 h interval from 2006 to 2018 into a precipitation dataset with a 1 h time scale. Based on this dataset, the eight evaluation indicators are applied to assess GPM at the grid points of the 15 rainfall stations, and the results are presented in Figure 5.

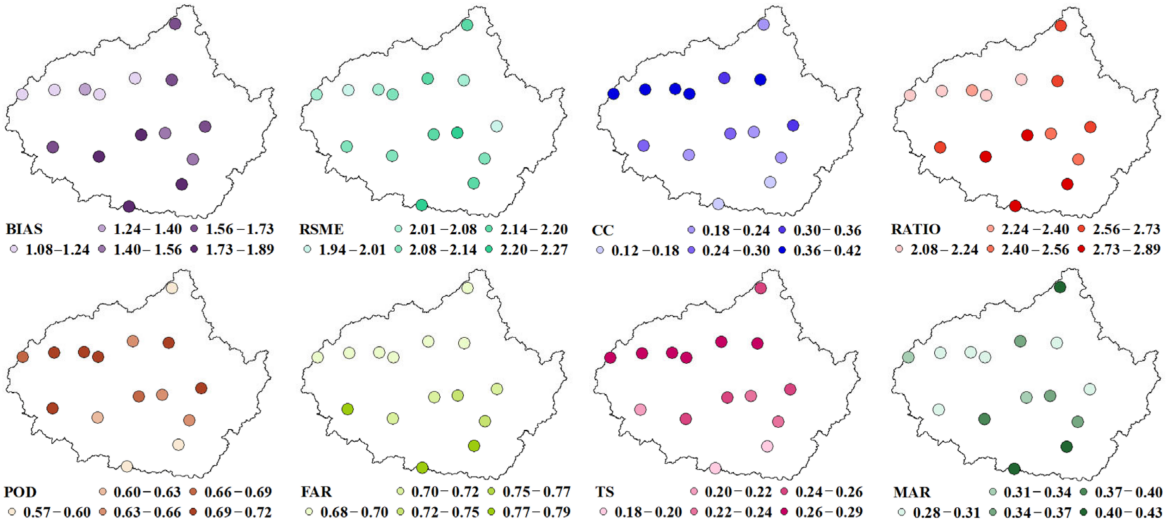

Figure 5. Evaluation of GPM with reference to rain gauge observations.

According to the quantitative evaluation results, on the whole, GPM overestimates rainfall events by approximately twice as much as the ground observations. The *BIAS* between GPM and gauge observation is greater than 1, and the *RATIO* is between 2 and 3. The *RSME* value does not vary significantly among gauges—mostly between 2 and 2.2 mm. In contrast, the *CC* varies widely among different gauges, with values ranging from 0.1 to 0.45. Qilijie station has the lowest *CC* value of 0.117, while Cao Dun station has the highest *CC* value of 0.422.

Regarding the categorical evaluation index results, the POD of GPM varies from 0.55 to 0.73 at each rainfall gauge, with an average value of 0.661. This indicates that approximately 66% of actual rainfall events can be captured and reflected by GPM. The *FAR* of GPM is around 0.7, which means that about 70% of the rainfall events observed by GPM are false alarms, i.e., no actual rainfall occurs. The *MAR* of GPM varies between 0.25 and 0.45 at each station, suggesting that approximately 30% of actual rainfall events correspond to GPM data of 0. It is important to note that individual classification index evaluation can be one-sided, and high *POD* may coincide with high *FAR*. *TS* integrates the evaluation of GPM on both hit and missed rainfall events, with an average value of 0.247 across all stations.

Overall, GPM data can partially reflect the actual rainfall patterns. However, there is an overall tendency to overestimate rainfall events, as well as omissions and the misreporting of some events, which indicates that the GPM data lacks stability.

4.2. Accuracy Evaluation of Different Models

4.2.1. Accuracy Evaluation at Rain Gauges

The accuracy evaluations of different precipitation data at the location of rain gauges during the training and testing stages are presented in Table 3. As can be seen from the table, for the training stage, FS-ConvLSTM exhibits superiority over other models in most indicators, except for two evaluation indicators related to total rainfall, including *BIAS* and *RATIO*, where F-SVD demonstrates better accuracy. For the testing stage, the advantage of FS-ConvLSTM is maintained, but LSTM shows better accuracy in *BIAS* and *RATIO*.

The evaluation results of different precipitation data show consistent performance in the training and testing stages.

Table 3. Performance of the FS-ConvLSTM fusion model in the training and testing stages.

Period	Data	*BIAS*	*RSME*	*CC*	*RATIO*	*POD*	*FAR*	*TS*	*MAR*
Training stage	GPM	1.029	3.874	0.295	2.029	0.524	0.496	0.346	0.476
	IDW	−0.036	1.998	0.489	0.964	0.552	0.326	0.436	0.448
	F-SVD	−0.027	1.481	0.753	0.973	0.634	0.186	0.554	0.366
	LSTM	−0.049	2.070	0.393	0.951	0.507	0.455	0.356	0.493
	FS-ConvLSTM	0.208	1.410	0.782	1.208	0.644	0.183	0.563	0.356
Testing stage	GPM	1.088	3.656	0.290	2.088	0.519	0.533	0.326	0.481
	IDW	−0.022	1.957	0.437	0.978	0.508	0.370	0.391	0.492
	F-SVD	−0.024	1.487	0.714	0.976	0.602	0.221	0.514	0.398
	LSTM	0.020	2.007	0.330	1.020	0.482	0.499	0.326	0.518
	FS-ConvLSTM	0.256	1.404	0.754	1.256	0.612	0.219	0.522	0.388

For the evaluation results of the quantitative indicators, the GPM data show an apparent overestimation. The ground-interpolated data slightly underestimate the rainfall, and the accuracy of F-SVD is better than that of IDW in each indicator value since the interpolation accounts for both spatial relationships and the trend of temporal changes. LSTM has lower *BIAS*, and *RATIO* is closer to 1, while FS-ConvLSTM has lower *RSME* and higher *CC*. Through fusing the data from rain gauges, the bias of GPM is improved, and the variation process fits better with the measured values. Compared with GPM, FS-ConvLSTM and LSTM reduce by 63.6% and 46.6% in *RSME* and improve by 165% and 33.2% in *CC*, respectively. Regarding the evaluation results of the categorical indicators, F-SVD shows obvious advantages over IDW, with higher *POD* and *TS* and lower *FAR* and *MAR*. The performance of LSTM is similar to that of GPM, while FS-ConvLSTM shows a great improvement in each indicator compared to GPM and LSTM. FS-ConvLSTM has the most accurate description of rainfall events, capturing and reflecting more than 60% of the rainfall events while reducing the cases of rainfall misreporting and omission. Compared with GPM, FS-ConvLSTM improves by 22.9% and 62.7% in *POD* and *TS* and is reduced by 63.1% and 25.2% in *FAR* and *MAR*. In summary, FS-ConvLSTM performs optimally in the description of rainfall variation process and event capture capability via the fusion of variation characteristics in the time and space of GPM and ground-interpolated rainfall data.

To compare the accuracy of rainfall data at different magnitudes more precisely, an accuracy evaluation was performed separately for light, medium, heavy, and torrential rainfall events during the testing stage, and the results are shown in Table 4. In light rainfall events, F-SVD performs best in the evaluation results of quantitative indicators, showing obvious advantages in *BIAS*, *RSME*, and *RATIO*. GPM performs best in the classification evaluation indicators, with the highest *POD* and *TS* and the lowest *MAR*. However, there is an apparent overestimation of rainfall in GPM, with values close to 3.8 times the measured values. In addition, FS-ConvLSTM has the highest *CC* and the lowest *FAR* among the models, which also indicates superiority. For the medium, heavy, and torrential rainfall events, FS-ConvLSTM has the lowest *RSME*, *FAR*, *MAR*, and the highest *CC*, *POD*, and *TS*, demonstrating that the spatiotemporal fusion data are closest to the variation process of the measured rainfall series and capture the rainfall events most accurately. Meanwhile, the ground-interpolated data performed best on *BIAS* and *RATIO* and are closest to the actual in terms of total rainfall.

Table 4. Evaluation results of the precipitation data in different types of rainfall events.

Type	Data	*BIAS*	*RSME*	*CC*	*RATIO*	*POD*	*FAR*	*TS*	*MAR*
Small rain	GPM	2.829	1.461	0.251	3.829	0.423	0.704	0.211	0.577
	IDW	−0.053	0.378	0.483	0.947	0.088	0.226	0.085	0.912
	F-SVD	−0.016	0.278	0.751	0.984	0.215	0.078	0.210	0.785
	LSTM	1.509	0.651	0.207	2.509	0.383	0.687	0.208	0.617
	FS-ConvLSTM	0.764	0.333	0.753	1.764	0.157	0.044	0.156	0.843
Moderate rain	GPM	0.970	2.317	0.151	1.970	0.381	0.629	0.232	0.619
	IDW	−0.020	1.469	0.247	0.980	0.332	0.470	0.256	0.668
	F-SVD	−0.011	1.102	0.649	0.989	0.463	0.277	0.394	0.537
	LSTM	0.323	1.447	0.214	1.323	0.329	0.595	0.222	0.671
	FS-ConvLSTM	0.463	1.018	0.724	1.463	0.464	0.262	0.398	0.536
Heavy rain	GPM	1.176	3.641	0.273	2.176	0.557	0.515	0.350	0.443
	IDW	−0.021	1.949	0.409	0.979	0.544	0.350	0.420	0.456
	F-SVD	−0.023	1.535	0.674	0.977	0.618	0.212	0.530	0.382
	LSTM	0.260	1.983	0.306	1.260	0.517	0.485	0.348	0.483
	FS-ConvLSTM	0.263	1.456	0.718	1.263	0.634	0.208	0.543	0.366
Torrential rain	GPM	1.063	4.903	0.314	2.063	0.594	0.475	0.386	0.406
	IDW	−0.024	2.477	0.485	0.976	0.623	0.334	0.475	0.377
	F-SVD	−0.027	1.846	0.748	0.973	0.708	0.209	0.602	0.292
	LSTM	−0.161	2.594	0.364	0.839	0.571	0.445	0.391	0.429
	FS-ConvLSTM	0.153	1.753	0.778	1.153	0.722	0.197	0.608	0.278

As the rainfall magnitude becomes larger, LSTM and FS-ConvLSTM are closer to the measured value in total rainfall; *BIAS* keeps decreasing, with *RATIO* becoming closer to 1. Since there is a direct relationship between *RSME* and rainfall magnitude, the *RSME* of the fused data also keeps increasing. The *CC* of FS-ConvLSTM fluctuates around 0.75, with the highest value of 0.778 for torrential rainfall events, while the *CC* of LSTM fluctuates between 0.2 and 0.4, becoming larger as the rainfall magnitude increases. In terms of classification indicators, as the rainfall event changes from light to heavy, the *POD* and *TS* of the fused data show an overall increasing trend, and the *MAR* and *FAR* also show an overall decreasing trend, suggesting that the rainfall capture capability keeps improving, and the FS-ConvLSTM performs better than the LSTM.

In general, FS-ConvLSTM exhibits advantages over other methods in rainfall events of different magnitudes, and its accuracy improves with the increase in rainfall magnitude.

4.2.2. Uncertainty Analysis

The estimation uncertainty of 15 rain gauges in each event during the testing stage was calculated, and box-line plots were generated to depict the distribution, as illustrated in Figure 6.

Based on the evaluation results of the quantitative indicators, the *BIAS* and *RATIO* of most precipitation data have a narrow error distribution interval, with a value around 1. In the case of light rain, the deviation of GPM is relatively larger, and the uncertainty interval wider compared to other data. The accuracy of the ground-interpolated data is slightly higher than that of the fused data, but this advantage decreases with increasing rainfall magnitude. FS-ConvLSTM has a smaller interval width than LSTM, which denotes higher stability. Regarding *RSME*, GPM has the highest median error in different magnitudes of rainfall, while F-SVD has a lower median value than IDW but with a larger interval width. The same difference exists between FS-ConvLSTM and LSTM, with the gap increasing as the magnitude of rainfall becomes larger. In terms of *CC*, the median values of GPM and LSTM are lower, while the median value of FS-ConvLSTM is the highest. F-SVD has a higher median value than IDW.

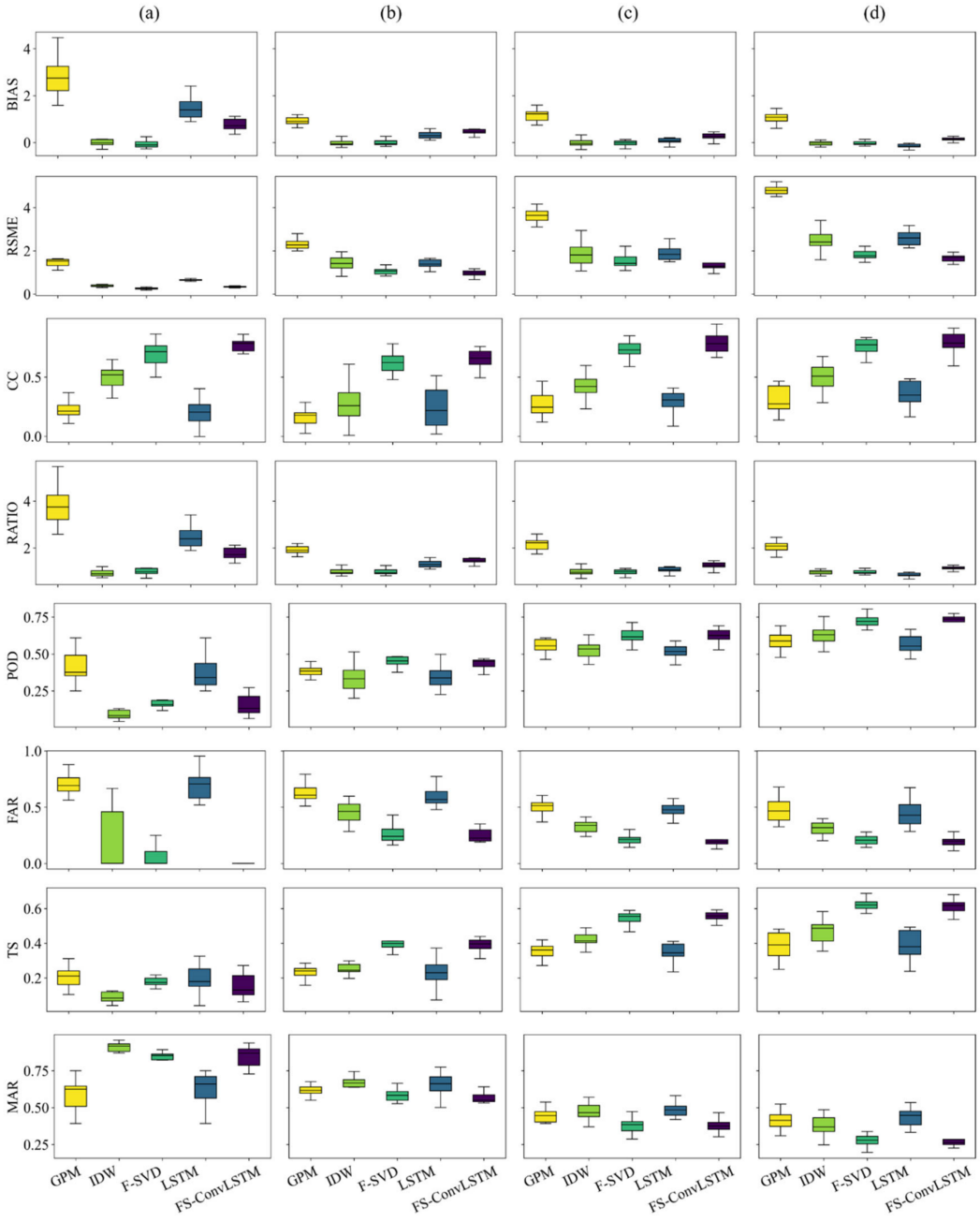

Figure 6. Boxplot of the evaluation indicators for different rainfall events. (**a**) Small rain; (**b**) Moderate rain; (**c**) Heavy rain; (**d**) Torrential rain.

Among the classification indicators, the values of *POD* and *TS* increase, and the values of *FAR* and *MAR* decrease as the rainfall magnitude increases. In light rainfall events, *POD*, *FAR*, and *MAR* exhibit large uncertainties. For ground-interpolated data, F-SVD has a better median and interval width of indicators than IDW. For the fused data, the median indicator of FS-ConvLSTM is generally better than LSTM, except in the light rainfall events where the median values of *POD*, *TS*, and *MAR* are worse for FS-ConvLSTM. As the rainfall magnitude changes from moderate to heavy rainfall, the difference between FS-ConvLSTM and LSTM in *POD* and *TS* increases while the difference in *FAR* decreases. FS-ConvLSTM also has a shorter interval width, indicating higher stability.

Based on the above analysis, FS-ConvLSTM shows better median accuracy than GPM and outperforms ground interpolation data and LSTM in most cases. The distribution width of FS-ConvLSTM is narrower than that of F-SVD and, in most cases, is narrower than

that of the GPM. Overall, FS-ConvLSTM improves both the accuracy and the stability of the rainfall data.

4.3. Model Performance in Typical Rainfall Events

4.3.1. Comparison of Temporal Variation Processes

Four typical rainfall events were chosen during the testing stage, and the variation patterns of rainfall observed by rain gauges, GPM, spatiotemporal interpolation by F-SVD, and the spatiotemporal fused data by FS-ConvLSTM were compared. The results are displayed in Figure 7.

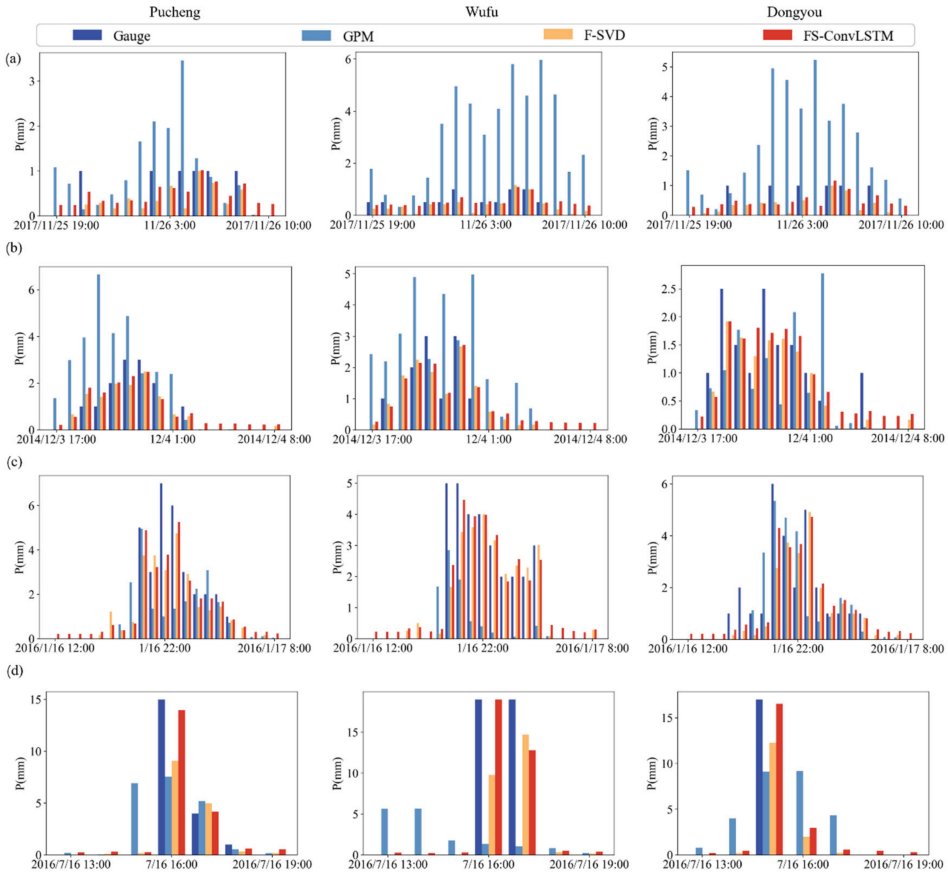

Figure 7. Comparison of the temporal variation process at three selected rain gauges. (**a**) Small rain; (**b**) Moderate rain; (**c**) Heavy rain; (**d**) Torrential rain.

From Figure 7a, it is evident that, for the light rainfall events, the rainfall intensities at all moments are below 1 mm/h. All types of rainfall data accurately capture the rainfall events, but there are differences in rainfall magnitudes. The GPM overestimates the rainfall significantly at all three stations, and the data of F-SVD and FS-ConvLSTM are closer to the actual measured values, with the fused data slightly higher than the ground observations. Notably, at Pucheng station, the value of FS-ConvLSTM is larger than that of F-SVD at the time of approaching the rain peak. Figure 7b shows that for the medium rainfall event, the rainfall intensity is below 3 mm/h at all moments. All three types of data reflect the rainfall event accurately, but GPM poorly describes the rain peak present time, and the rain peak at Pucheng station is earlier than the actual measurement, while the rain peak at Dongyou station is later than the actual measurement, showing considerably more uncertainty. At most moments, GPM is higher than the actual measurement, and the data of F-SVD and FS-ConvLSTM are slightly lower than the actual measurement. For the peak of rainfall, the values of FS-ConvLSTM are closer to the measured values compared to F-SVD. Figure 7c shows that, for heavy rainfall events, the maximum rainfall intensity is around 6 mm/h.

At Pucheng and Wufu stations, GPM appears to underestimate the rainfall, and the rainfall variation trend reflected at Pucheng station lags behind the measured data. Both the F-SVD and FS-ConvLSTM data accurately reflect the magnitudes and trends of the rainfall, but overall, FS-ConvLSTM performs better than F-SVD. Finally, Figure 7d illustrates that, for torrential rainfall events, the maximum rainfall intensity is above 15 mm/h. GPM underestimates the rainfall events, and the capture of rainfall trends at the Wufu station is also biased. There is also a slight underestimation in F-SVD for the rain peaks, and the rain peaks of FS-ConvLSTM are closer to the measured values than F-SVD.

After analyzing the four different magnitudes of rainfall events, it can be concluded that GPM is less reliable in describing the rainfall magnitude. The data tend to overestimate rainfall for light and moderate rainfall events while underestimating rainfall for heavy and torrential rain. On the other hand, F-SVD provides a more accurate description of rainfall magnitudes and rainfall trends, despite underestimating the rainfall peaks. FS-ConvLSTM outperforms F-SVD in accurately reflecting the rainfall events, particularly in rainfall peaks, which is more evident in heavy and torrential rainfall events.

4.3.2. Comparison of the Spatial Distribution

During the testing stage, two rainfall events of different magnitudes were selected, and their cumulative rainfall spatial distributions were plotted. The resulting figures (Figures 8 and 9) show the distribution of GPM, F-SVD, and FS-ConvLSTM from left to right.

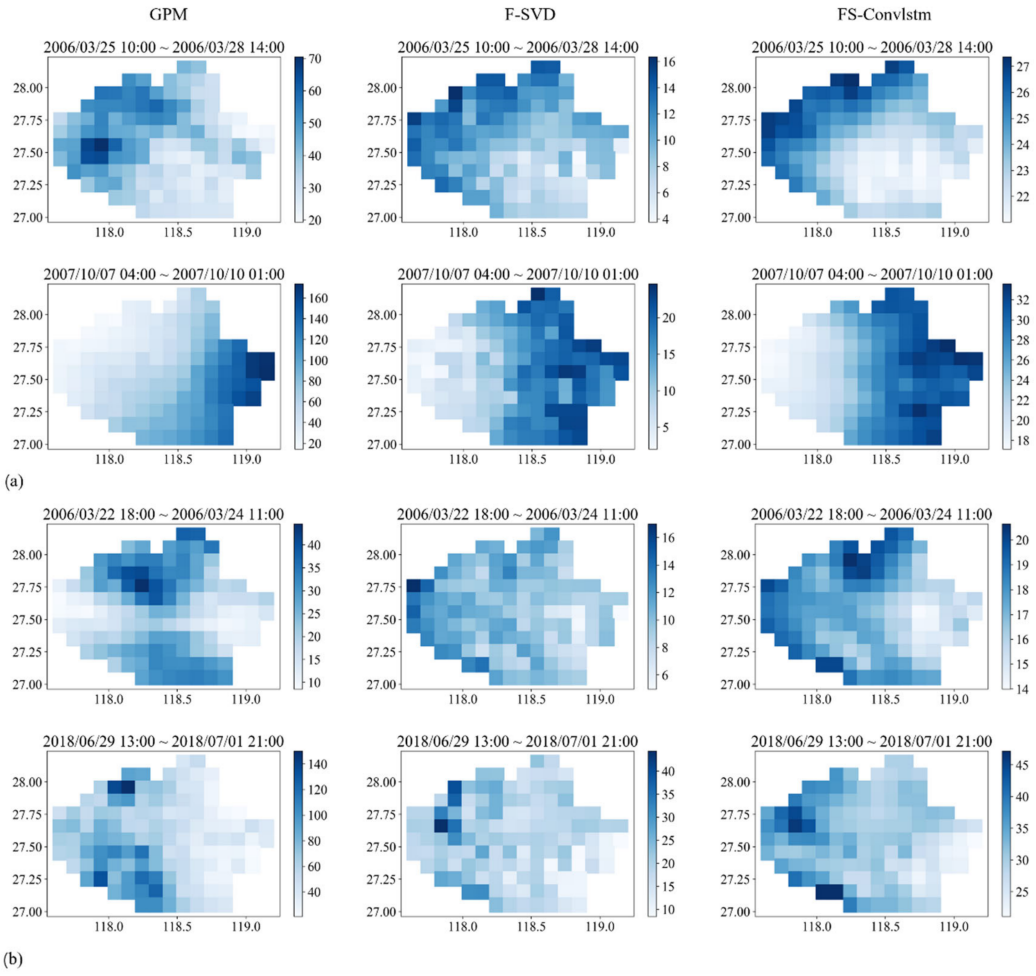

Figure 8. Spatial distribution of the accumulated precipitation for small and moderate rainfall events. (**a**) Small rain; (**b**) Moderate rain.

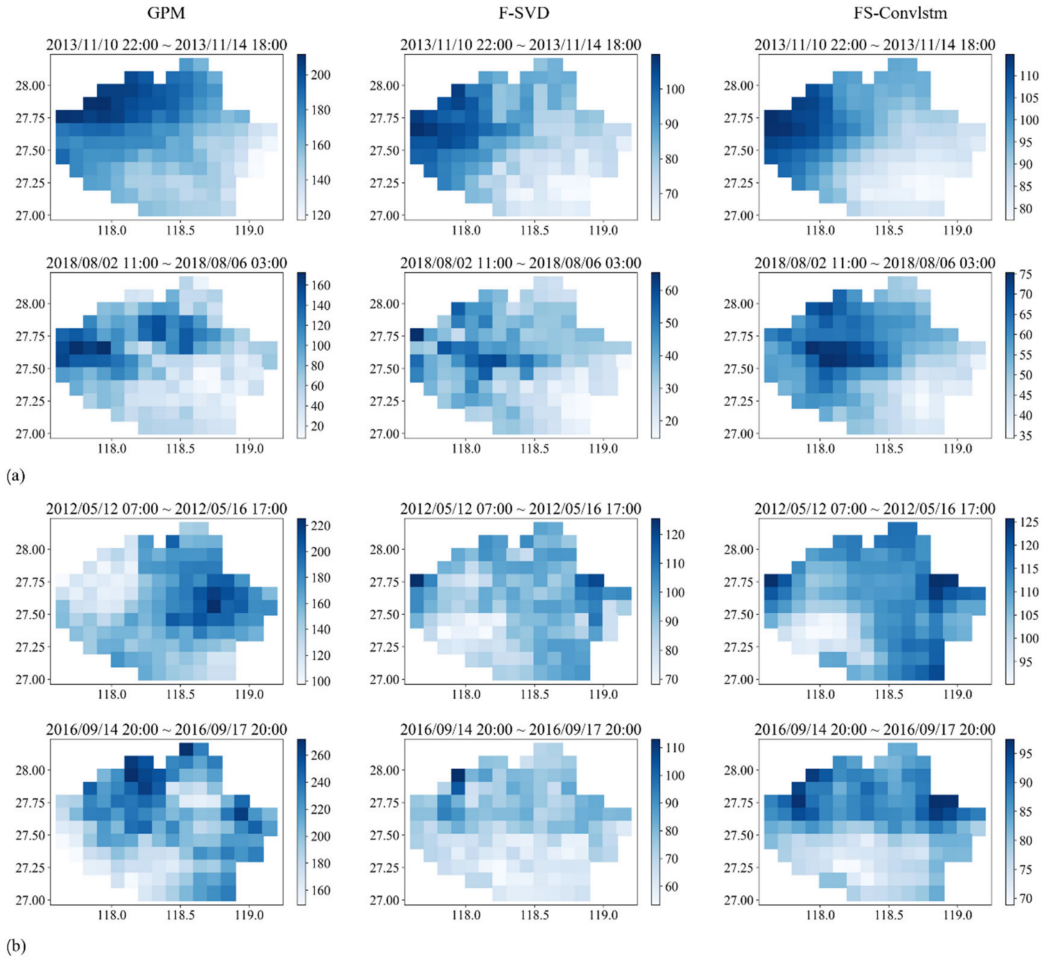

Figure 9. Spatial distribution of the accumulated precipitation for heavy and torrential rainfall events. (**a**) Heavy rain; (**b**) Torrential rain.

As seen in Figure 8a, the rainfall epoch for light rainfall events is around 3 days. The values of F-SVD and FS-ConvLSTM are closer, while the magnitude of the GPM data is significantly larger. For spatial extreme values of accumulated rainfall, the minimal values of FS-ConvLSTM and the minimal values of GPM are closer, and the maximal values of FS-ConvLSTM are slightly larger than those of F-SVD. GPM and FS-ConvLSTM are more continuous in spatial variation, while F-SVD has multiple isolated points in space that can produce abrupt changes in rainfall amounts. The rainfall centers of GPM and F-SVD are slightly different in space, and the rainfall centers of the two data and the rainfall distribution of the surrounding points are reflected in the fusion data. Similar results are found for the medium rainfall event, as seen in Figure 8b, where the duration of the medium rainfall event is around two days. The magnitude of GPM estimation is higher than the other two data, and the spatial extremes of F-SVD and FS-ConvLSTM are very close. The spatial distributions of the three data are relatively similar, but the values for F-SVD are more discrete in terms of spatial variation compared to the continuous spatial variation of GPM and FS-ConvLSTM. The fused data combine the distribution characteristics of GPM and F-SVD, with the spatial aggregation of rainfall of both reflected in the fusion.

For heavy rainfall events, as depicted in Figure 9a, the rainfall duration lasts for approximately four days. GPM continues to overestimate the rainfall magnitude, while the magnitudes of F-SVD and FS-ConvLSTM are closer and the spatial extremes are similar. The spatial distribution of rainfall reflected by GPM and F-SVD are similar, and the location of the rainfall center is also close, corresponding to a similar distribution in the fused data. FS-ConvLSTM shows better spatial continuity. As for the torrential rainfall events, as shown

in Figure 9b, the rainfall duration is about 3–4 days. Regarding rainfall magnitude, GPM is relatively large compared to the other two types of data. In terms of spatial distribution, F-SVD shows abrupt changes, and the rainfall at a few points is significantly higher than at other surrounding points, resulting in poor spatial continuity. Moreover, GPM and F-SVD have single and multiple rainfall centers, respectively, and the distribution of both rainfall centers is reflected in the fusion.

In general, GPM exhibits continuous spatial distribution but overestimates rainfall events. F-SVD shows abrupt spatial variations but is more accurate in its response to magnitude. FS-ConvLSTM combines the advantages of GPM in spatial distribution and the advantages of F-SVD in magnitude, which display continuous spatial distribution and closely approximate the actual rainfall values.

5. Discussion

The proposed FS-ConvLSTM framework effectively merges hourly precipitation data from rain gauge and GPM observations, resulting in improved accuracy and reduced uncertainty when estimating spatial precipitation. The framework's ability to capture the precipitation variation process and its superior performance compared to alternative models highlight its potential for practical application in precipitation estimation.

The comparison results presented in Table 3 and Figure 6 demonstrate that the proposed FS-ConvLSTM outperforms LSTM in terms of accuracy and stability. While traditional LSTM models only consider time-series dependencies, ConvLSTM combines the strengths of LSTM and convolutional neural networks (CNN), allowing it to effectively capture spatiotemporal dependencies and model both temporal and spatial dimensions [27]. Additionally, traditional LSTM primarily relies on matrix multiplication and element-wise operations [28], which limits its capacity to model data nonlinearly. In contrast, by utilizing multiple filters and the local connectivity of the convolution kernel, ConvLSTM can learn richer feature representations and extract more complex spatiotemporal patterns in the data. These characteristics contribute to the improved accuracy and stability of FS-ConvLSTM observed in the comparison results.

Comparing the fusion results of FS-ConvLSTM for different magnitudes of rainfall data (Table 4, Figures 6 and 7), it can be observed that the fusion results for heavy rainfall are better. Heavy rains exhibit stronger spatial and temporal correlation and spatial expansion, whereas small rains tend to be more localized and discrete. The convolution operation in ConvLSTM utilizes shared weights across different spatial locations [29], enabling it to effectively capture the spatial characteristics of heavy rainfall. Furthermore, heavy rainfall events have longer durations, and past rainfall conditions can influence future rainfall. The gating mechanism and memory units in ConvLSTM aid the model in retaining and updating key spatiotemporal information [30], facilitating the capture of long-term dependencies associated with heavy rainfall. These capabilities of ConvLSTM contribute to its superior performance in understanding and fusing heavy rainfall data.

From the spatial distribution of the rainfall data before and after fusion presented in Figures 8 and 9, it is evident that the fusion process retains the distribution features of both data sources while achieving higher accuracy. The introduction of multiple input channels in the ConvLSTM model enables the simultaneous processing of inputs from multiple data sources [31]. This allows the model to leverage the strengths of each data source, capture their spatial features, and retain the expression of these features in the fusion results. Moreover, the ConvLSTM model exhibits a large capacity and nonlinear modeling capability, enabling it to effectively handle the heterogeneity and nonlinear correlation between different data sources during the fusion process [32]. The model learns adaptively and adjusts the weights based on the importance and contribution of each data source. This ability enables the model to identify and reduce the impact of data with large deviations on the accuracy of fusion results, resulting in more accurate outcomes.

While the proposed framework successfully merges precipitation data from satellites and rain gauges, it has certain limitations. The ConvLSTM method was chosen for this

study due to its ability to capture spatial and temporal dependencies in rainfall data, but alternative deep learning models such as Transformer-based models may also have advantages in processing spatiotemporal structured data. Exploring and comparing the performance of different architectures for precipitation data fusion would be a valuable direction for future research. Additionally, it is important to note that the framework proposed in this paper was tested in a single study region with a dense network of rain gauges in southeast China, so expanding the study area and incorporating data from additional stations would provide a more comprehensive understanding of the framework's performance across a larger spatial extent.

6. Conclusions

This study proposes an integrated framework (FS-ConvLSTM) to spatiotemporally merge precipitation data from rain gauge observations and GPM (IMERG V06). The proposed framework integrates F-SVD in the recommender system to improve the accuracy of spatiotemporal interpolation based on rain gauge observations, and ConvLSTM merges precipitation data from satellites and rain gauge interpolations by exploiting the spatiotemporal correlation pattern between them. The FS-ConvLSTM framework was applied to estimate the hourly spatial precipitation in the Jianxi Basin of China from 2006 to 2018. The findings are summarized as follows:

(1) The proposed FS-ConvLSTM framework outperforms the comparative models (IDW, F-SVD, and LSTM) in terms of precipitation variation process description and rainfall capture capability, reducing the *RSME* and *FAR* of the original GPM data by 63.6% and 63.1%, respectively, and increasing the *CC* and *POD* by 165% and 22.9%, respectively.
(2) The merged data not only improve the accuracy of the precipitation but also reduce the uncertainty in precipitation estimation. As the intensity of precipitation increases, the precipitation capture ability substantially improves, and the estimation more closely matches the measured data in terms of total rainfall.
(3) Due to the powerful feature extraction capability of ConvLSTM, the merged precipitation data combines the advantages of GPM and ground interpolation data with the continuous spatial distribution data and values close to the actual one, and the spatial aggregation of both data is reflected in the fusion.

The two-step merging framework proposed in this study demonstrates satisfactory performance in merging hourly spatial precipitation data in the Jianxi basin of China by exploring the spatiotemporal dependence between rain gauge and GPM. Different types of precipitation data, such as Tropical Rainfall Measuring Mission (TRMM), the Precipitation Estimation from Remotely Sensed Information using Artificial Neural Networks (PERSIANN), and the Climate Hazards Group InfraRed Precipitation with Station (CHIRPS), possess their unique characteristics and advantages. In this study, we only considered merging data from rain gauges and GPM. To maximize the benefits of each satellite product's data and enhance the accuracy of spatial precipitation estimations, future work should consider incorporating more multi-source precipitation observation data.

Author Contributions: Conceptualization, S.S. and H.C.; methodology, S.S., H.C. and K.L.; software, S.S. and K.L.; validation, S.S., N.Z. and B.T.; formal analysis, S.S.; investigation, N.Z. and B.T.; resources, S.S. and K.L.; data curation, N.Z., B.T. and K.L.; writing—original draft preparation, S.S.; writing—review and editing, H.C. and C.-Y.X.; visualization, S.S.; supervision, H.C. and C.-Y.X.; project administration, K.L.; funding acquisition, H.C. All authors have read and agreed to the published version of the manuscript.

Funding: This research was funded by the National Key Research and Development Program (2022YFC3002701) and Water Science and Technology Project in Fujian Province, China.

Data Availability Statement: The rain gauge observation data used in this study are confidential and the GPM (IMERG V06) Final Run data were downloaded from NASA (https://earthdata.nasa.gov/; accessed on 15 October 2022).

Conflicts of Interest: The authors declare no conflict of interest.

References

1. Hinge, G.; Hamouda, M.A.; Long, D.; Mohamed, M.M. Hydrologic utility of satellite precipitation products in flood prediction: A meta-data analysis and lessons learnt. *J. Hydrol.* **2022**, *612*, 128103. [CrossRef]
2. Estébanez-Camarena, M.; Taormina, R.; van de Giesen, N.; ten Veldhuis, M.-C. The Potential of Deep Learning for Satellite Rainfall Detection over Data-Scarce Regions, the West African Savanna. *Remote Sens.* **2023**, *15*, 1922. [CrossRef]
3. Song, J.-H.; Her, Y.; Kang, M.-S. Estimating Reservoir Inflow and Outflow From Water Level Observations Using Expert Knowledge: Dealing With an Ill-Posed Water Balance Equation in Reservoir Management. *Water Resour. Res.* **2022**, *58*, e2020WR028183. [CrossRef]
4. Talchabhadel, R.; Shah, S.; Aryal, B. Evaluation of the Spatiotemporal Distribution of Precipitation Using 28 Precipitation Indices and 4 IMERG Datasets over Nepal. *Remote Sens.* **2022**, *14*, 5954. [CrossRef]
5. Ramanathan, A.; Versini, P.A.; Schertzer, D.; Perrin, R.; Sindt, L.; Tchiguirinskaia, I. Stochastic simulation of reference rainfall scenarios for hydrological applications using a universal multi-fractal approach. *Hydrol. Earth Syst. Sci.* **2022**, *26*, 6477–6491. [CrossRef]
6. Gofa, F.; Flocas, H.; Louka, P.; Samos, I. A Coherent Approach to Evaluating Precipitation Forecasts over Complex Terrain. *Atmosphere* **2022**, *13*, 1164. [CrossRef]
7. Gyasi-Agyei, Y. A framework for comparing two rainfields based on spatial structure: A case of radar against selected satellite precipitation products over southeast Queensland, Australia. *J. Hydrol.* **2022**, *613*, 128356. [CrossRef]
8. Sreeparvathy, V.; Srinivas, V.V. A Bayesian Fuzzy Clustering Approach for Design of Precipitation Gauge Network Using Merged Remote Sensing and Ground-Based Precipitation Products. *Water Resour. Res.* **2022**, *58*, e2021WR030612. [CrossRef]
9. Noor, R.; Arshad, A.; Shafeeque, M.; Liu, J.; Baig, A.; Ali, S.; Maqsood, A.; Pham, Q.B.; Dilawar, A.; Khan, S.N.; et al. Combining APHRODITE Rain Gauges-Based Precipitation with Downscaled-TRMM Data to Translate High-Resolution Precipitation Estimates in the Indus Basin. *Remote Sens.* **2023**, *15*, 318. [CrossRef]
10. Iqbal, Z.; Shahid, S.; Ahmed, K.; Wang, X.; Ismail, T.; Gabriel, H.F. Bias correction method of high-resolution satellite-based precipitation product for Peninsular Malaysia. *Theor. Appl. Clim.* **2022**, *148*, 1429–1446. [CrossRef]
11. Varouchakis, E.A.; Kamińska-Chuchmała, A.; Kowalik, G.; Spanoudaki, K.; Graña, M. Combining Geostatistics and Remote Sensing Data to Improve Spatiotemporal Analysis of Precipitation. *Sensors* **2021**, *21*, 3132. [CrossRef]
12. Papacharalampous, G.; Tyralis, H.; Doulamis, A.; Doulamis, N. Comparison of Tree-Based Ensemble Algorithms for Merging Satellite and Earth-Observed Precipitation Data at the Daily Time Scale. *Hydrology* **2023**, *10*, 50. [CrossRef]
13. Chen, S.; Li, Q.; Zhong, W.; Wang, R.; Chen, D.; Pan, S. Improved Monitoring and Assessment of Meteorological Drought Based on Multi-Source Fused Precipitation Data. *Int. J. Environ. Res. Public Health* **2022**, *19*, 1542. [CrossRef]
14. Yumnam, K.; Kumar Guntu, R.; Rathinasamy, M.; Agarwal, A. Quantile-based Bayesian Model Averaging approach towards merging of precipitation products. *J. Hydrol.* **2022**, *604*, 127206. [CrossRef]
15. Shao, Y.; Fu, A.; Zhao, J.; Xu, J.; Wu, J. Improving quantitative precipitation estimates by radar-rain gauge merging and an integration algorithm in the Yishu River catchment, China. *Theor. Appl. Clim.* **2021**, *144*, 611–623. [CrossRef]
16. Pan, Y.; Yuan, Q.; Ma, J.; Wang, L. Improved Daily Spatial Precipitation Estimation by Merging Multi-Source Precipitation Data Based on the Geographically Weighted Regression Method: A Case Study of Taihu Lake Basin, China. *Int. J. Environ. Res. Public Health* **2022**, *19*, 13866. [CrossRef]
17. Duan, Z.; Ren, Y.; Liu, X.; Lei, H.; Hua, X.; Shu, X.; Zhou, L. A comprehensive comparison of data fusion approaches to multi-source precipitation observations: A case study in Sichuan province, China. *Environ. Monit. Assess.* **2022**, *194*, 422. [CrossRef]
18. Lei, H.; Zhao, H.; Ao, T. A two-step merging strategy for incorporating multi-source precipitation products and gauge observations using machine learning classification and regression over China. *Hydrol. Earth Syst. Sci.* **2022**, *26*, 2969–2995. [CrossRef]
19. Zhang, J.; Xu, J.; Dai, X.; Ruan, H.; Liu, X.; Jing, W. Multi-Source Precipitation Data Merging for Heavy Rainfall Events Based on Cokriging and Machine Learning Methods. *Remote Sens.* **2022**, *14*, 1750. [CrossRef]
20. Zhang, Z.; Wang, D.; Qiu, J.; Zhu, J.; Wang, T. Machine Learning Approaches for Improving Near-Real-Time IMERG Rainfall Estimates by Integrating Cloud Properties from NOAA CDR PATMOS-x. *J. Hydrometeorol.* **2021**, *22*, 2767–2781. [CrossRef]
21. Shen, J.; Liu, P.; Xia, J.; Zhao, Y.; Dong, Y. Merging Multisatellite and Gauge Precipitation Based on Geographically Weighted Regression and Long Short-Term Memory Network. *Remote Sens.* **2022**, *14*, 3939. [CrossRef]
22. Wu, H.; Yang, Q.; Liu, J.; Wang, G. A spatiotemporal deep fusion model for merging satellite and gauge precipitation in China. *J. Hydrol.* **2020**, *584*, 124664. [CrossRef]
23. Shi, X.; Chen, Z.; Wang, H.; Yeung, D.-Y.; Wong, W.-K.; Woo, W.-C. Convolutional LSTM network: A machine learning approach for precipitation nowcasting. *Adv. Neural Inf. Process. Syst.* **2015**, *28*, 802–810.
24. Chen, H.; Sheng, S.; Xu, C.-Y.; Li, Z.; Zhang, W.; Wang, S.; Guo, S. A spatiotemporal estimation method for hourly rainfall based on F-SVD in the recommender system. *Environ. Modell. Softw.* **2021**, *144*, 105148. [CrossRef]
25. Durrani, A.u.R.; Minallah, N.; Aziz, N.; Frnda, J.; Khan, W.; Nedoma, J. Effect of hyper-parameters on the performance of ConvLSTM based deep neural network in crop classification. *PLoS ONE* **2023**, *18*, e0275653. [CrossRef]

26. Hu, W.S.; Li, H.C.; Pan, L.; Li, W.; Tao, R.; Du, Q. Spatial–Spectral Feature Extraction via Deep ConvLSTM Neural Networks for Hyperspectral Image Classification. *IEEE Trans. Geosci. Remote Sens.* **2020**, *58*, 4237–4250. [CrossRef]
27. Dizaji, M.S.; Mao, Z.; Haile, M. A hybrid-attention-ConvLSTM-based deep learning architecture to extract modal frequencies from limited data using transfer learning. *Mech. Syst. Signal Process.* **2023**, *187*, 109949. [CrossRef]
28. Zhang, W.; Ge, F.; Cui, C.; Yang, Y.; Zhou, F.; Wu, N. Design and Implementation of LSTM Accelerator Based on FPGA. In Proceedings of the 2020 IEEE 20th International Conference on Communication Technology (ICCT), Nanning, China, 28–31 October 2020; pp. 1675–1679.
29. De Medrano, R.; Aznarte, J.L. On the inclusion of spatial information for spatio-temporal neural networks. *Neural Comput. Appl.* **2021**, *33*, 14723–14740. [CrossRef]
30. Li, Y.; Chai, S.; Wang, G.; Zhang, X.; Qiu, J. Quantifying the Uncertainty in Long-Term Traffic Prediction Based on PI-ConvLSTM Network. *IEEE Trans. Intell. Transp. Syst.* **2022**, *23*, 20429–20441. [CrossRef]
31. Eide, S.S.; Riegler, M.A.; Hammer, H.L.; Bremnes, J.B. Deep Tower Networks for Efficient Temperature Forecasting from Multiple Data Sources. *Sensors* **2022**, *22*, 2802. [CrossRef]
32. Zhang, X.; Zhou, Y.n.; Luo, J. Deep learning for processing and analysis of remote sensing big data: A technical review. *Big Earth Data* **2022**, *6*, 527–560. [CrossRef]